JGR Oceans

RESEARCH ARTICLE
10.1029/2018JC014635

The Dominant Global Modes of Recent Internal Sea Level Variability

B. D. Hamlington[1], S. H. Cheon[2], C. G. Piecuch[3], K. B. Karnauskas[4], P. R. Thompson[5], K.-Y. Kim[6], J. T. Reager[1], F. W. Landerer[1], and T. Frederikse[1]

[1]Jet Propulsion Laboratory, California Institute of Technology, Pasadena, CA, USA, [2]Department of Ocean, Earth and Atmospheric Sciences, Old Dominion University, Norfolk, VA, USA, [3]Physical Oceanography Department, Woods Hole Oceanographic Institution, Woods Hole, MA, USA, [4]Department of Atmospheric and Oceanic Sciences and Cooperative Institute for Research in Environmental Sciences, University of Colorado Boulder, Boulder, CO, USA, [5]Department of Oceanography, University of Hawai'i at Manoa, Honolulu, HI, USA, [6]School of Earth and Environmental Sciences, Seoul National University, Seoul, South Korea

Key Points:
- Intraseasonal to decadal variability has a significant impact on global and regional sea level
- The modern observing system provides the opportunity to separate contributions on intraseasonal to decadal timescales
- By finding the dominant modes of recent sea level variability, an improved understanding of regional and global sea level is obtained

Correspondence to:
B. D. Hamlington,
benjamin.d.hamlington@jpl.nasa.gov

Citation:
Hamlington, B. D., Cheon, S. H., Piecuch, C. G., Karnauskas, K. B., Thompson, P. R., Kim, K.-Y., et al. (2019). The dominant global modes of recent internal sea level variability. *Journal of Geophysical Research: Oceans*, *124*, 2750–2768. https://doi.org/10.1029/2018JC014635

Received 4 OCT 2018
Accepted 19 MAR 2019
Accepted article online 21 MAR 2019
Published online 23 APR 2019

Abstract The advances in the modern sea level observing system have allowed for a new level of knowledge of regional and global sea level in recent years. The combination of data from satellite altimeters, Gravity Recovery and Climate Experiment (GRACE) satellites, and Argo profiling floats has provided a clearer picture of the different contributors to sea level change, leading to an improved understanding of how sea level has changed in the present and, by extension, may change in the future. As the overlap between these records has recently extended past a decade in length, it is worth examining the extent to which internal variability on timescales from intraseasonal to decadal can be separated from long-term trends that may be expected to continue into the future. To do so, a combined modal decomposition based on cyclostationary empirical orthogonal functions is performed simultaneously on the three data sets, and the dominant shared modes of variability are analyzed. Modes associated with the trend, seasonal signal, El Niño–Southern Oscillation, and Pacific decadal oscillation are extracted and discussed, and the relationship between regional patterns of sea level change and their associated global signature is highlighted.

1. Introduction

In the context of understanding and preparing for future sea level change, internal climate variability plays two primary roles: (1) it serves to obscure the background anthropogenic trend in sea level, particularly in short data records, and (2) it causes an increase or decrease in regional and global sea level on short timescales that can temporarily ameliorate or exacerbate the effects of long-term sea level rise. In recent years, many studies have investigated these two roles, seeking to separate and quantify the sea level variability associated with a variety of large-scale modes of climate variability (e.g., Bromirski et al., 2011; Cazenave et al., 2014; Hamlington et al., 2013, 2014, 2015; Han et al., 2017; Moon et al., 2015, 2013; Palanisamy et al., 2015; Piecuch & Quinn, 2016; Sreenivas et al., 2012; Zhang & Church, 2012). In doing so, there is the potential to both uncover the long-term trend that may be expected to persist into the future and provide an assessment of the envelope of possible sea level change on shorter planning horizons. An approach in these studies is to perform statistical analysis focusing on a particular timescale of interest, comparing the results to indices used to track large-scale climate modes or even using these indices as part of the analysis (e.g., Bromirski et al., 2011; Piecuch & Quinn, 2016; Zhang & Church, 2012; broadly summarized in Han et al., 2017). Particular focus has been placed on intraseasonal to decadal timescales, over which regional mean sea level is dominated by basin-scale ocean-atmosphere modes of internal climate variability.

While the approach of using climate indices to attribute regional sea level variability to a specific process or signal is informative and productive in many cases including in those studies mentioned above, it can lead to potential problems on occasion (e.g., Kenigson & Han, 2018). First, most internal climate modes are not independent and are connected to each other via atmospheric teleconnections and common centers of action (e.g., Alexander et al., 2002; Deser et al., 2004; Newman et al., 2016). For example, the Pacific decadal oscillation (PDO), Arctic Oscillation, Pacific North American pattern, and even the El Niño–Southern Oscillation (ENSO) are all associated with variability in the position and/or intensity of the Aleutian Low pressure system. Variability in the Aleutian Low forces a substantial fraction of open-ocean and coastal

sea level change in the North Pacific, and as a result, each mode is associated with a pattern of sea level change that is spatially and temporally correlated with patterns associated with the other modes (Alexander et al., 2002; Deser et al., 2004; Newman et al., 2003; Zhang & Church, 2012). This correlation makes it difficult to decide which modes best represent sea level variability in a given region and can often lead to assigning a certain physical explanation when another may be more accurate. Secondly, the temporal evolution of internal climate modes is generally quantified using statistically derived and defined indices of sea surface temperature (SST; e.g., Mantua & Hare, 2002) or sea level pressure. Such indices provide useful indicators of past and present climate states, but they are less useful as forward looking metrics that can be used for planning and decision-making. Surface variables, such as SST and sea level pressure, respond to a variety of processes and tend to be dominated by higher-frequency variability. As a result, predicting the temporal evolution of these indices is difficult. Lastly, when obvious agreement to known climate signals is not present and supported by comparison to climate indices, meaningful results can be rejected or ignored.

Rather than relying on predefined climate modes to form the basis of our understanding of intraseasonal to decadal sea level variability, we can take a nonparametric approach (i.e., not relying on climate indices) to understanding and assessing regional and global sea level change on these timescales. This approach can be extended to include other observations in order to identify links between the large-scale variability in sea level and other components of the Earth climate system. Specifically, in this paper, we seek to find the dominant modes of variability in sea level and understand how these modes contribute to regional and global sea level on their inherent timescales. With the modern observational network over the past two decades, it is now possible to apply a comprehensive multivariate approach toward understanding the variability in the sea level record. As a result, the focus here is on modern observational records, including those with relatively short record lengths and with trends that are potentially heavily impacted by variability on intraseasonal to decadal timescales. In doing so, insight can be gained on the role the water cycle plays in sea level variability (Cazenave et al., 2014; Hamlington et al., 2017; Reager et al., 2016), the extent to which terrestrial water storage (TWS) varies in response to large-scale climate variability (e.g., Boening et al., 2012; Fasullo et al., 2013), and the relative roles of steric and mass-driven variability to changes in regional and global sea level (Cazenave et al., 2018; Piecuch & Quinn, 2016). While not specifically relying on comparisons to climate indices, the general approach taken here does not preclude links or attribution to well-known climate signals like ENSO or the PDO. Among the questions we seek to answer or provide additional insight into are as follows:

1. What are the dominant signals or modes characterizing sea level change on intraseasonal to decadal timescales?
2. To what extent does internal variability obscure the background trend in satellite records, both regionally and globally?
3. What contributes to the short-term rise and fall of global mean sea level?
4. What role does variability in the water cycle play in changes in sea level, particularly on global scales?
5. Are satellite records of terrestrial water storage now long enough to extract long-term trends regionally and globally?

These questions have been the focus of a number of recent papers that have resulted in important insights into the role of intraseasonal to decadal variability in sea level (e.g., Boening et al., 2012; Cazenave et al., 2014; Fasullo et al., 2013; Fasullo & Nerem, 2016; Hamlington et al., 2013, 2014, 2015, 2016; Reager et al., 2016; Zhang & Church, 2012). This study differs primarily by not targeting a particular climate signal a priori and instead simultaneously looking for dominant modes that are shared across data sets. We then seek to understand these modes using information from the different contributors to sea level change and consider the available record lengths of those contributors. Finally, we try to put these results in the context of other investigations into intraseasonal to decadal variability in sea level and indeed the broader climate system.

2. Data

Recent studies have shown the ability to close the "sea level budget" on global scales using a combination of satellite altimetry, Argo profiling floats and the Gravity Recovery and Climate Experiment (GRACE) satellites (Cazenave et al., 2018). These observing systems provide measurements of total, steric, and land water storage, respectively. Here we take advantage of this network and seek to extract common modes of

variability across the three data sets. Further comparisons are made to precipitation and sea surface temperature (SST) data or provide support in the interpretation of the returned modes. The data sets used will be detailed below, but some preprocessing steps are common to all data sets. Specifically, in order to perform the modal analysis on each set of data simultaneously, it is necessary to interpolate to the same steps in time. We choose monthly time steps, which are sufficient for the analysis of intraseasonal to decadal variability. Also, a spatial map of the time mean value at each grid cell is removed from each data set. Nothing else is done to the data beyond these two steps, with the trend and seasonal cycle both left intact and allowed to influence the resulting modes of the statistical analysis.

2.1. Satellite Altimetry

For satellite altimetry data, we use the Jet Propulsion Laboratory MEaSUREs gridded sea surface height anomaly data set that is part of the Integrated Multi-Mission Ocean Altimeter Data for Climate Research. Specifically, these are gridded sea surface height anomalies above a mean sea surface on 1/6th degree grid every 5 days. As mentioned above, the data are converted to monthly time steps and the spatial grid is coarsened to a half-degree grid to match the spatial resolution of the other data sets. The gridded data use the sea surface height anomalies of TOPEX/Poseidon, Jason-1, Jason-2, and Jason-3 as the reference data and supplement with data from several other satellite altimeters. The time period covered is from 1993 to present, although we only use data through 2016 to match available observations from other data sets.

2.2. Argo Steric Sea Level

Monthly Argo in situ temperature and salinity grids produced by Scripps Institution of Oceanography (SIO) are used to compute steric sea level. Other data sets beyond the SIO product are available for this purpose, and recent studies have shown some differences between these data sets (e.g., Dieng et al., 2017). However, these differences are small during the time period considered here, and as a check the analysis performed was repeated with other steric sea level data sets with little discernible difference. The grids are generated using objective analysis applied to quality-controlled float profiles (Roemmich & Gilson, 2009). The monthly grids with half-degree horizontal resolution span from 65°S to 65°N and cover depths down to 2,000 m but do not have global coverage due to lack of sufficient sampling in marginal seas. Further, contributions from below 2,000 m are not accounted for here but may explain some of the discrepancies when analyzing global mean contributions. Data covering the time period between 2004 and 2016 are used. These gridded fields are used to evaluate steric sea level following Gill and Niiler (1973) and similar to the procedure in Piecuch and Quinn (2016).

2.3. GRACE Land Water Storage

To account for changes in land water storage, we used monthly gridded estimates of equivalent water thickness based on retrievals from the GRACE. Specifically, we used the mascon solutions from Release-05 data generated by the National Aeronautics and Space Administration Jet Propulsion Laboratory (Watkins & Yuan, 2012; Wiese et al., 2016). The data used here has half-degree spatial resolution and covers the time period from 2004 to 2016. The data were corrected for glacial isostatic adjustment prior to use. While GRACE does provide data over the ocean, we only use the land water storage data in an attempt to add to the discussion of recent papers that have detailed the relationship between the transfer of water between the land and the ocean and sea level as measured by altimetry on intraseasonal to decadal timescales. The analysis was repeated with ocean mass data from GRACE, and the results were found to be consistent with what is presented below in terms of the returned modes and the global contributions.

3. Methods

A wide range of techniques have been applied to extract or isolate intraseasonal to decadal sea level variability, including modal decompositions, windowed-trend analyses, and more straightforward comparisons between observations and climate indices. While each method has its merits, here we employ cyclostationary empirical orthogonal function (CSEOF) analysis to find the dominant modes of variability in the data sets of interest (Kim et al., 2015). CSEOFs have been used extensively for exactly this purpose in recent years, with applications to sea surface temperature, winds, precipitation, and sea level, among other state variables (Hamlington et al., 2011, 2014; Kim et al., 2015; Mason et al., 2017; Yeo & Kim, 2013). The justification for using CSEOFs is twofold: (1) the goal is to find the dominant modes of variability without targeting a specific

climate signal making a modal decomposition appropriate (this goal could be met with most types of empirical orthogonal function (EOF)-based analysis) and (2) CSEOFs allow for temporally lagged covariation between different climate variables that may be otherwise difficult to extract. This last point is particularly important when simultaneously analyzing multiple variables. There is an expectation, for example, that a change in precipitation would precede a change in TWS suggesting that a single spatial pattern for each variable that is modulated by a shared time series would be inadequate to understand the inherent relationship. As a further example more applicable to the current study should not be assumed that steric and mass-driven contributions to global mean sea level occur in phase and the possibility of a lag should be allowed for.

One limitation to CSEOF analysis is the need to select a nested period prior to performing the analysis (more details below). We rely, however, on previous studies to make this choice (e.g., Hamlington et al., 2016; Yeo & Kim, 2013). Presenting CSEOFs as a superior choice to other analysis techniques is not a specific goal of this paper, and we state that our interpretation of the returned modes is likely influenced by the use of CSEOFs. When compared to an EOF decomposition, however, CSEOFs hold a number of benefits. For example, EOFs do not accommodate spatiotemporal varying signals in a single mode. In an EOF description, a mode has a single pattern that is ascribed a particular amplitude that changes through time. The pattern itself does not change. That means that a single mode cannot capture propagating features. Instead, a series of modes are required to explain climate variability that evolves or has propagating features, with the seasonal signal being a particularly important example. Additionally, as discussed above, a combined EOF decomposition of different variables would obscure possible phase differences between the variables. A number of other statistical analyses that are more appropriate for capturing periodic or quasi-periodic signals were applied to these same data sets with mixed and varied although largely consistent results in terms of the final interpretation of the variability in these data sets. Both extended EOFs and complex EOFs have been explored, but CSEOFs are found to be easier to interpret and understand in the present case, in part because of their previous application to the same data sets. It is possible that there are other more suitable or equally suitable analysis techniques, which we recognize by commenting here.

As mentioned above, CSEOF analysis has been discussed and used to study climate variability. For the benefit of the reader, a brief overview of CSEOFs is provided here (a more detailed explanation is in Kim et al., 2015). The CSEOF method decomposes space-time data into a series of modes comprised a spatial component (known hereafter as the loading vector [LV]) and a corresponding temporal component (known hereafter as the principal component time series [PCTS]). The main difference between CSEOF and the more widely used EOF analysis is the LVs' time dependence, which allows the spatial pattern of each CSEOF mode to vary in time, with the temporal evolution of the spatial pattern of the CSEOF LVs constrained to be periodic with a selected "nested period". In other words, space-time data ($T(r,t)$) is defined as

$$\begin{aligned} T(r,\ t) &= \sum_i \mathrm{LV}_i(r,\ t)\mathrm{PC}_i(t) \\ \mathrm{LV}(r,\ t) &= \mathrm{LV}(r,\ t\ +\ d) \end{aligned} \tag{1}$$

where the loading vectors are time dependent and are periodic with the nested period, d. As a result, each CSEOF mode is composed of 12 LVs and 1 PCTS when, for example, using monthly data and a 1-year nested period. In other words, the temporal evolution related to an inherent physical process is captured in the LV, while the corresponding PCTS explains the amplitude of this physical process through time. The nested period of the CSEOF analysis is selected a priori, with the decision usually based on some physical understanding or intuition regarding the data to be studied. By increasing the size of the nested period, the number of maps in the resulting LVs also increases.

CSEOF analysis has previously been applied to satellite altimetry-measured sea level using both a 1-year and a 2-year nested period (Hamlington et al., 2011, 2016). Both nested periods return similar modes for the annual cycle (maps of the LV repeated twice in the case of a 2-year nested period). With a 2-year nested period and a long enough record, however, it is possible to separate a biennial oscillation associated with ENSO from lower-frequency variability often attributed to the PDO. Given its quasi-periodic nature, we recognize that ENSO does exhibit variability that does not simply transition between cold and warm phases on biennial timescales. An example of this is the quasi-quadrennial variability that has been the subject of many past studies and most recently summarized in Timmermann et al. (2018). As a test, a 4-year nested period was also applied. The returned modes did not significantly change from those presented below, and there was

no mode obviously varying on quadrennial timescales. Such temporal variability will be captured in the PCTS rather than explained with evolving LVs, or possibly represented in a different mode. Further, CSEOFs do have a windowing effect that occurs at the end points, and as a general rule, the smallest justifiable nested period should be used to minimize this potential issue. Following the lead of past studies and with the relatively short time period of the records considered here, we use a 2-year nested period here with the goal of separating the trend and annual cycle into separate modes and targeting the biennial oscillation in ENSO as a starting point. The choice of nested period does not remove any particular type of signal in the resulting analysis and instead provides a structure to ideally improve interpretation of the variability in the data set. The biggest impact of this structure is whether the physical period is represented in the LV or in the PCTS. In the case where the physical period is much longer than the nested period, for example, the oscillation between phases of a given signal will be captured in the PCTS with the LVs appearing relatively constant over the given nested period. This will also be true of any representation of a trend in the data set.

As stated previously, the purpose here is to take advantage of the extent of the modern sea level observing system to capture and understand the dominant multivariate modes of variability. We perform a combined CSEOF analysis, simultaneously decomposing total sea level (satellite altimetry), mass-driven sea level (GRACE), and steric sea level (Argo). Expressed in terms of more traditional statistical analysis, this is analogous to a coupled singular value decomposition with the additional structure imposed by the cyclostationary framework incorporated. By searching for shared modes of variability across the three data sets, the objective is to provide a clearer picture of the processes contributing to regional and global sea level on timescales of interest. It also serves the purpose of understanding the role that natural variability may play in changes to the water cycle. There have also been several recent studies investigating the causes of nonseasonal variations in global mean sea level (GMSL), particularly as related to ENSO. The approach adopted here serves to further the discussion of Piecuch and Quinn (2016; among others) that attempted to separate and estimate the relative ENSO-related steric and mass-driven effects on GMSL. Furthermore, with the GRACE record coming to an end recently, it is worth investigating the extent to which intraseasonal to decadal mass-driven sea level variability in the roughly 15-year record can be explained and understood. Supporting analysis is also provided by simultaneously decomposing sea level along with precipitation and SST, which provide longer record lengths and highlight problems associated with extracting decadal-scale variability from the relatively short Argo and GRACE records.

In summary, after interpolating the three data sets (satellite altimetry, Argo, and GRACE) to have consistent monthly temporal resolution and similar spatial resolutions, a CSEOF decomposition is performed using a 2-year nested period. Only the mean is removed from each data set with the trend and seasonal cycle left in to be separated by the CSEOF analysis. Each data set is in units of sea level (or equivalent sea level), and no additional normalization is performed on the data sets. This preserves the balance that is provided by the observations from GRACE and Argo approximately summing to the observations from satellite altimetry. When performing the combined analysis with sea level and either precipitation or SST; however, both data sets are normalized by their standard deviation prior to applying CSEOFs given the differing units on the data sets.

4. Results

4.1. Combined CSEOF Sea Level Analysis

To extract the dominant modes in sea level, a simultaneous CSEOF decomposition is performed on the satellite altimetry, Argo, and GRACE data covering the period from 2004 to 2016. Below, we discuss in detail the first four modes that explain 86% (37%, 28%, 11%, and 10%, respectively) of the variability in the combined data sets, with the vast majority (65%) contained in the first two modes.

4.1.1. Regional Trend Mode

The first mode of the decomposition as shown in Figure 1 primarily represents the trend in each data set. By trend, we do not refer to a linear increase as would be estimated by ordinary least squares. While this mode does incorporate much of the linear trend present in each of the data sets, there is some variability about the linear change. For ease of discussion in this paper, however, we refer to this mode as the "trend mode" as that is the prominent feature. This CSEOF mode and those that follow are shown with seasonal LVs for each of the three variables. Each LV initially contains 24 maps (one for each month of the 2-year nested period),

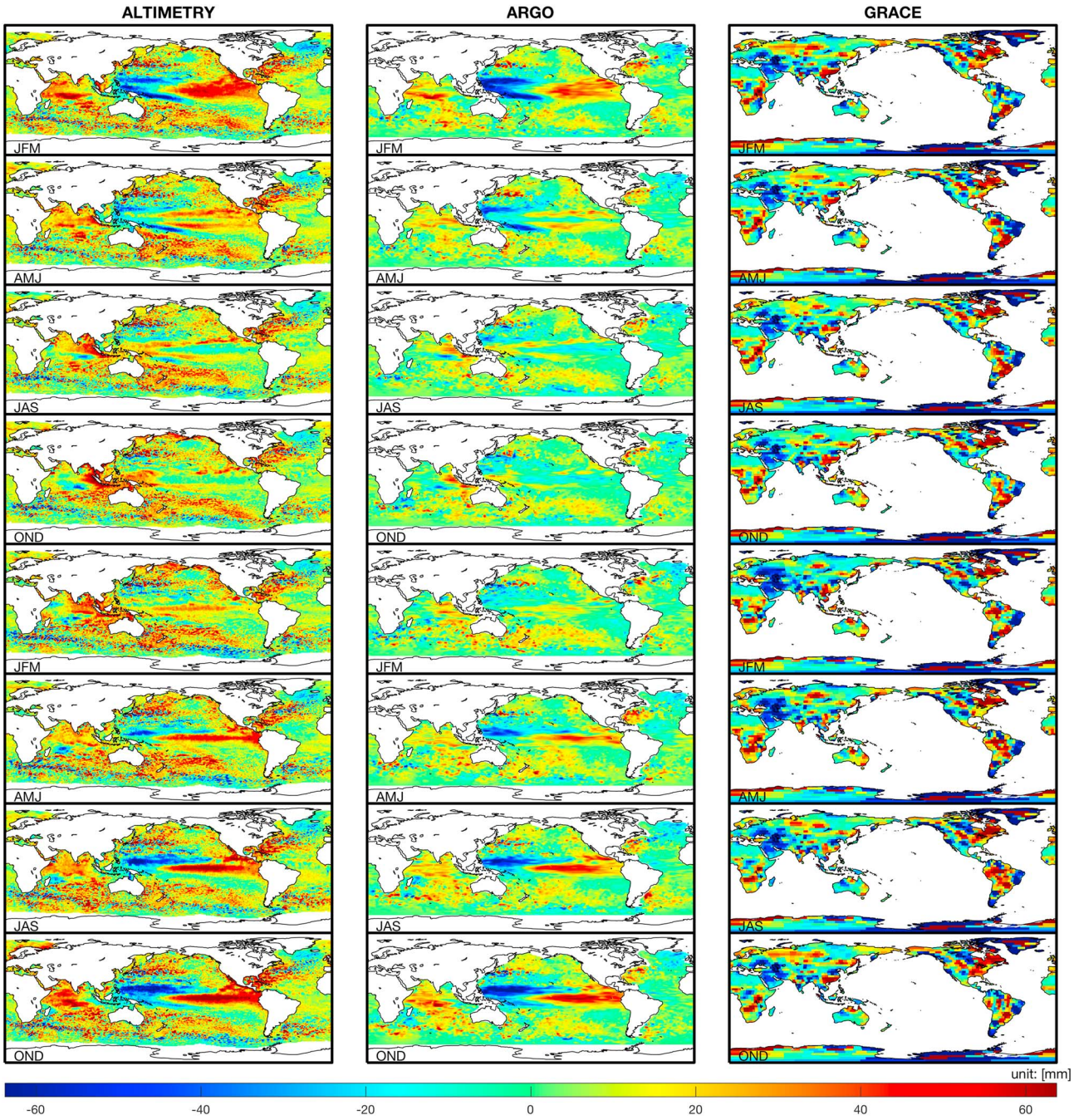

Figure 1. First CSEOF mode from the combined decomposition representing the trend in each of the three data sets. Seasonally averaged LVs are shown covering the 2-year nested period for altimetry (left), Argo (middle), and GRACE (right). CSEOF = cyclostationary empirical orthogonal function; GRACE = Gravity Recovery and Climate Experiment; JFM = January–March; AMJ = April–June; JAS = July–September; OND = October–December.

but for ease of display, these are averaged into seasonal maps for January/February/March, April/May/June, July/August/September, and October/November/December. While each variable has its own set of LVs, they share a single PCTS (Figure 2a), which can be combined with the LVs and averaged globally to compute the contribution of the mode to GMSL (Figures 2b and 2c). The start date of the analysis is January 2004, so the first year of each LV represents even-numbered years, while the last year represents odd-numbered years. Following the explanation above regarding the meaning of "trend" in this paper, the reason for interpretation of this mode as representing the trend is twofold: (1) most obviously, the PCTS shows a strong positive trend over the length of the record and (2) the LVs vary little over the 2-year

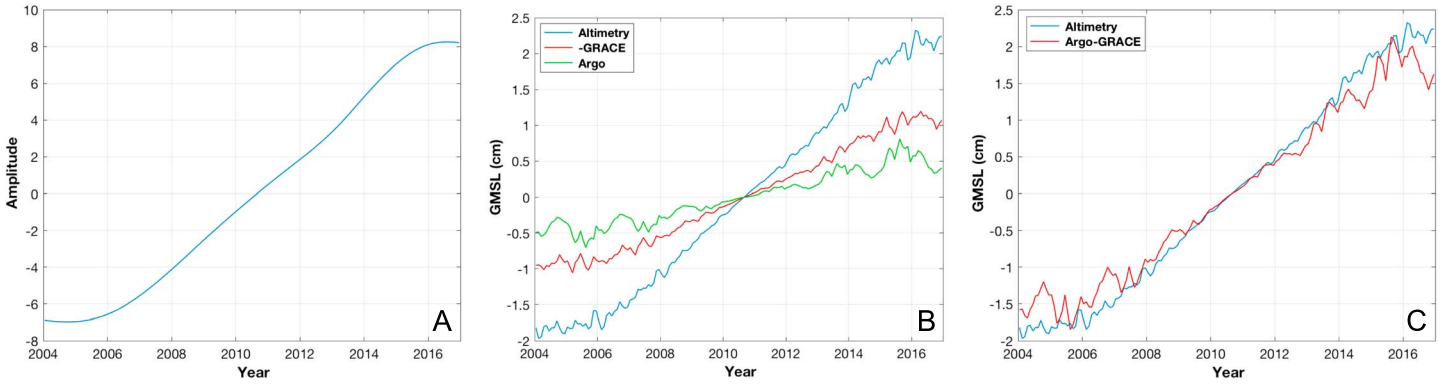

Figure 2. (a) PCTS associated with the trend mode in Figure 1 and (b) global mean time series computed by combining the CSEOF LV and PCTS and averaging spatially for each variable in the CSEOF trend mode. (c) The combination of Argo and GRACE compared to the total sea level measured by the altimetry. PCTS = principal component time series; CSEOF = cyclostationary empirical orthogonal function; LV = loading vector; GRACE = Gravity Recovery and Climate Experiment; GMSL = global mean sea level.

nested period, suggesting a period much longer than that chosen for the CSEOF decomposition. Consequently, we determine the sea level contribution from each mode and compute the linear trend to create a trend map for each of the variables (Figure 3, middle column). It should be noted that the flattening occurring at the boundaries of the PCTS is associated with the windowing associated with CSEOFs described above. For comparison, we also show the total trends in each data set (Figure 3, left column) before decomposing into modes and the difference between the total trends and CSEOF trend mode (Figure 3, right column). We submit that the difference map can be interpreted as those trends during the record that result from internal climate variability, although it should be noted that it is unlikely that it contains all internal climate variability. To explain further, if the trend mode (Figure 1) is capturing only the long-term trends in each data set, any regional trends that remain would be associated in part with the phasing of internal climate modes over the course of the record. This does not appear to exactly be the case as there is still considerable spatial variability in the trend mode from the CSEOF

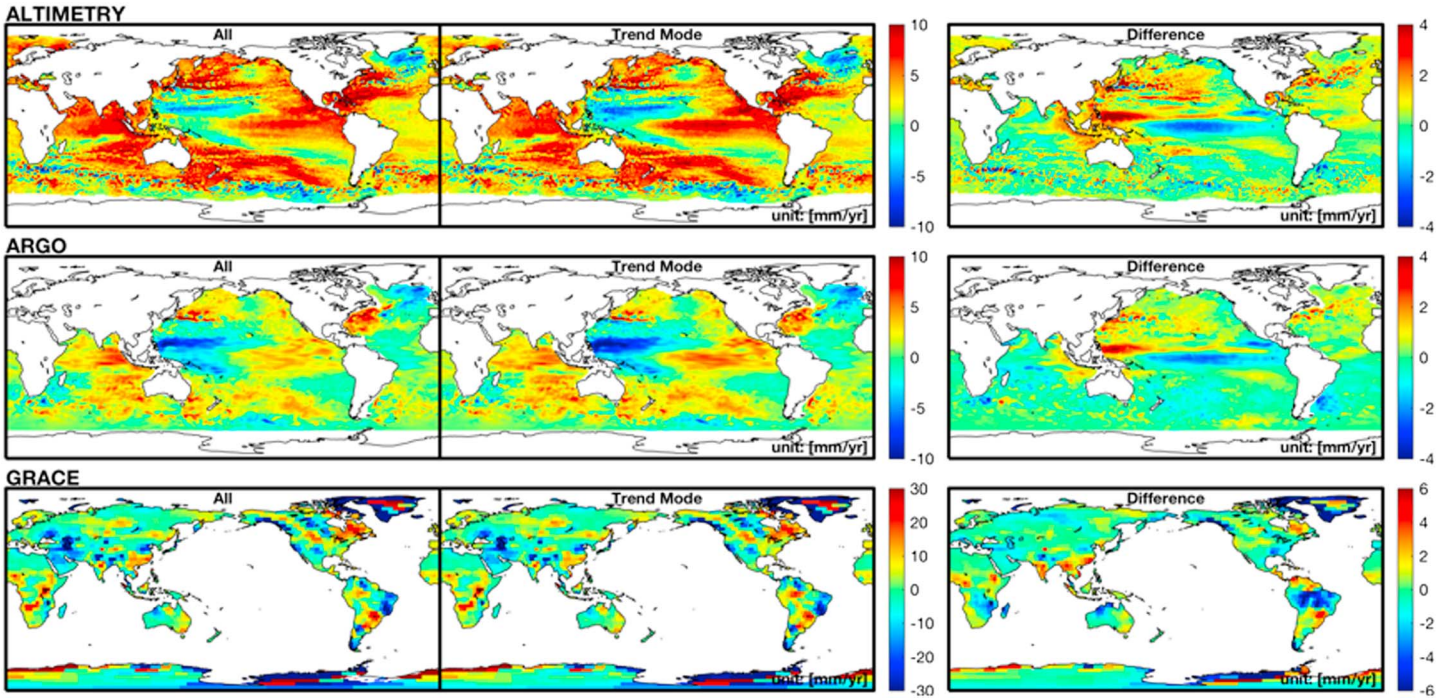

Figure 3. Regional trends (mm/year) from 2004 to 2016 from the complete data sets (left), the CSEOF trend mode as shown in Figure 1 (middle), and the difference between the total trends and the trend mode (right). CSEOF = cyclostationary empirical orthogonal function; GRACE = Gravity Recovery and Climate Experiment.

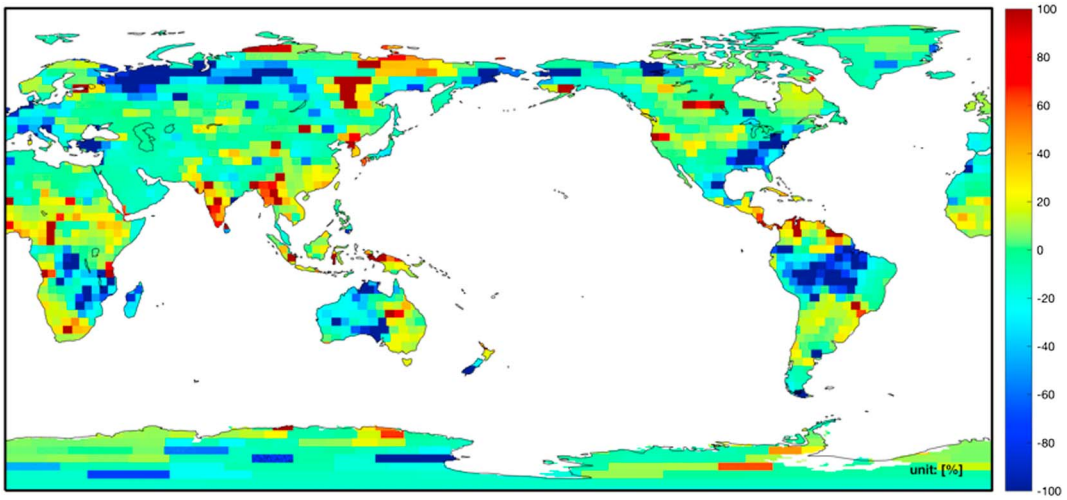

Figure 4. The differenced trend map from Figure 3 divided by the magnitude of the total trends to show the relative contribution of natural variability to the estimated trends.

decomposition, some of which is likely attributable to natural climate variability that is not separated. This is likely due to a combination of the technique and relatively short records used here, although there is also likely a spatial pattern associated with the forced trends in sea level that may account for some of this variability. In general, however, variability on the order of 13 years—the length of the data records—or longer will be difficult to distinguish from the estimated trend. We do see a number of notable features, however, when examining both the map associated with the trend mode and the difference map associated with internal climate variability. Much of the spatial variability in the altimeter trend map results from the steric trends with the difference between the two being a relatively smooth spatial field (not shown) owing to the regional mass-driven trends. The trends associated with natural variability are not obviously attributable to a specific signal in every area, although there is a strong negative trend in the central Pacific in both the total sea level and steric sea level maps, which is consistent with the persistent negative trend in the index tracking the El Niño Modoki (Ashok et al., 2007) over the same period of time. Trends in the region generally attributed to the PDO are small, mirrored by the similarly small trends in the PDO index (Mantua & Hare, 2002). In the Indian Ocean, the trends indicate a general shift from positive to negative phases in the Indian Ocean Dipole (IOD) over the course of the record, again reflected in the negative trend of the Dipole Mode Index (Sagi & Yamagata, 2003) that tracks the phases of the IOD.

The water mass trends from GRACE show some interesting features. Most of the areas experiencing ice mass loss are explained in the trend mode, with comparatively small trends in these areas attributed to natural variability. As a further demonstration of this, Figure 4 shows the differenced trend map (Figure 3, right column) divided by the magnitude of the total trends, showing more clearly that natural variability does not fully explain the trends associated with ice mass loss. Of particular note are mass losses in eastern Brazil, southeastern United States, northern Europe, western Australia, and the southeastern Africa, and mass gains in central India, southeast Asia, eastern Australia, the Nile headwaters, western tropical Africa, northern Great Plains, and northern and southern portions of Brazil. These results are in general agreement with the GRACE trends attributed to natural variability in Rodell et al. (2018), although it should be noted that there are a number of other areas with trends here that are not picked out as attributable to natural variability in the referenced study.

We can recombine the LV and PCTS and then spatially average to estimate the GMSL trends. Several previous studies have computed a GMSL "budget," determining if the combination of mass-driven trends from GRACE and steric trends from Argo match that of total sea level from satellite altimetry (Cazenave et al., 2018). We similarly check for such budget closure with the trend mode discussed here with the GMSL time series from each variable shown in Figure 2. From 2004 to 2016, the GMSL trend in total sea level from the trend mode is 3.19 mm/year, while the mass-driven and steric trends are 1.81 mm/year and 0.94 mm/year,

respectively, summing to 2.74 mm/year over the same time period. Most of the disagreement occurs at the endpoints of the time series, especially after 2016 when the sum of steric and mass-driven GMSL falls and the total sea level does not. Finally, in recombining the PCTS and LV to compute the GMSL time series, each data point in the PCTS is multiplied by a corresponding LV map. For January 2004, for example, the first point in the PCTS is multiplied by the global average of the January map of year 1 of the LV. When the PCTS approaches zero, the global contribution of the mode must all approach zero. For a purely linear temporal trend that is perfectly captured by a single CSEOF mode, the 24 LV maps in the trend mode would all have the same spatial pattern and the same global mean. In other words, the spatial pattern in the LV would not vary at all across the 2-year nested period. The degree to which this is not the case is visible at the ends of the time series, where the PCTS gets larger in magnitude and amplifies any deviations from a consistent value over the course of the 2-year LV. The smoothness of the GMSL time series in the interior of the time series and the fluctuations at the end points are thus both an artifact of the method and also informative as to the ability to capture the trend in the data sets.

4.1.2. Annual Mode

When investigating intraseasonal to decadal variability in sea level, a typical first step is to remove the annual cycle. Often the annual cycle is estimated through a harmonic fit, treated as having the same amplitude year after year. Other studies, however, have reported temporal variations in the amplitude of the annual cycle of sea level (Calafat et al., 2018; Hamlington et al., 2011). While occasionally overlooked, these year-to-year variations can serve to significantly increase the risk of coastal flooding by adding to the baseline of sea level upon which higher-frequency variability superimposes. Given the regular and defined period that can be targeted with the nested period, the CSEOF technique is particularly well suited to extract the annual cycle and its modulation in strength over time. Further, the ability of the CSEOFs to describe differences in phase among different variables is especially important when simultaneously decomposing steric, mass-driven and total sea level change.

The resulting CSEOF mode, the second after the trend mode, is shown in Figure 5. Again, the 24 monthly maps of the LV are averaged down to seasonal maps, four for each year. With a 2-year nested period, the annual cycle is repeated twice through the series of maps in the LV. The patterns for total and steric sea level are similar, with lower (higher) sea levels in the northern (southern) hemisphere during the beginning of the year and higher (lower) sea levels in the northern (southern) hemisphere in the latter half of the year. For the seasonal variations of water mass on land as measured by GRACE, a number of notable features are seen, including the transition from wet to dry season in both the Amazon Basin and Okavango Delta over the course of the year, and the seasonal monsoon in India with a rainy season in the latter half of the year. The accompanying PCTS (Figure 6a) provides information on the strength of the annual cycle over the course of the record. Compared to Hamlington et al. (2011), much smaller deviations—on the order of $\pm 5\%$—from the average are seen during the record. While attribution of the modulation in the strength of the annual cycle is not immediately obvious, the PCTS is anticorrelated with the PCTS for the subsequent ENSO-like biennial oscillation mode that will be discussed in more detail below. This suggests a suppression of the annual cycle during an El Niño and a strengthening of the annual cycle during a La Niña. Note that the strictly positive PCTS for the annual mode is able to meet the requirements for an orthogonal decomposition while still having a nonzero correlation with other modes.

As with the trend mode, we recombine the LVs and PCTS and estimate the contribution of this mode to GMSL, as shown in Figures 6b and 6c. The 1-year periodicity of this mode becomes obvious when averaging the maps in the LV. The seasonal cycle of the steric component is roughly half the amplitude of the annual variations in land mass. As discussed in Leuliette and Willis (2015), the steric sea level variations largely cancel between the Northern and Southern Hemispheres, with the greater ocean area in the Southern Hemisphere heating imparting the phasing on the global steric signal. Combining the out-of-phase contributions of the steric and mass components, we can again determine if budget closure is achieved for the annual CSEOF mode. As with the trend mode, there is still small disagreement between the total sea level annual cycle and that resulting from the combination of steric and water mass. There is agreement in phase, however, and unlike Leuliette and Willis (2015), no effort was made to remove areas that are covered by one set of observations and not the other. This likely explains much of the resulting disagreement and is consistent with the results in Piecuch and Quinn (2016).

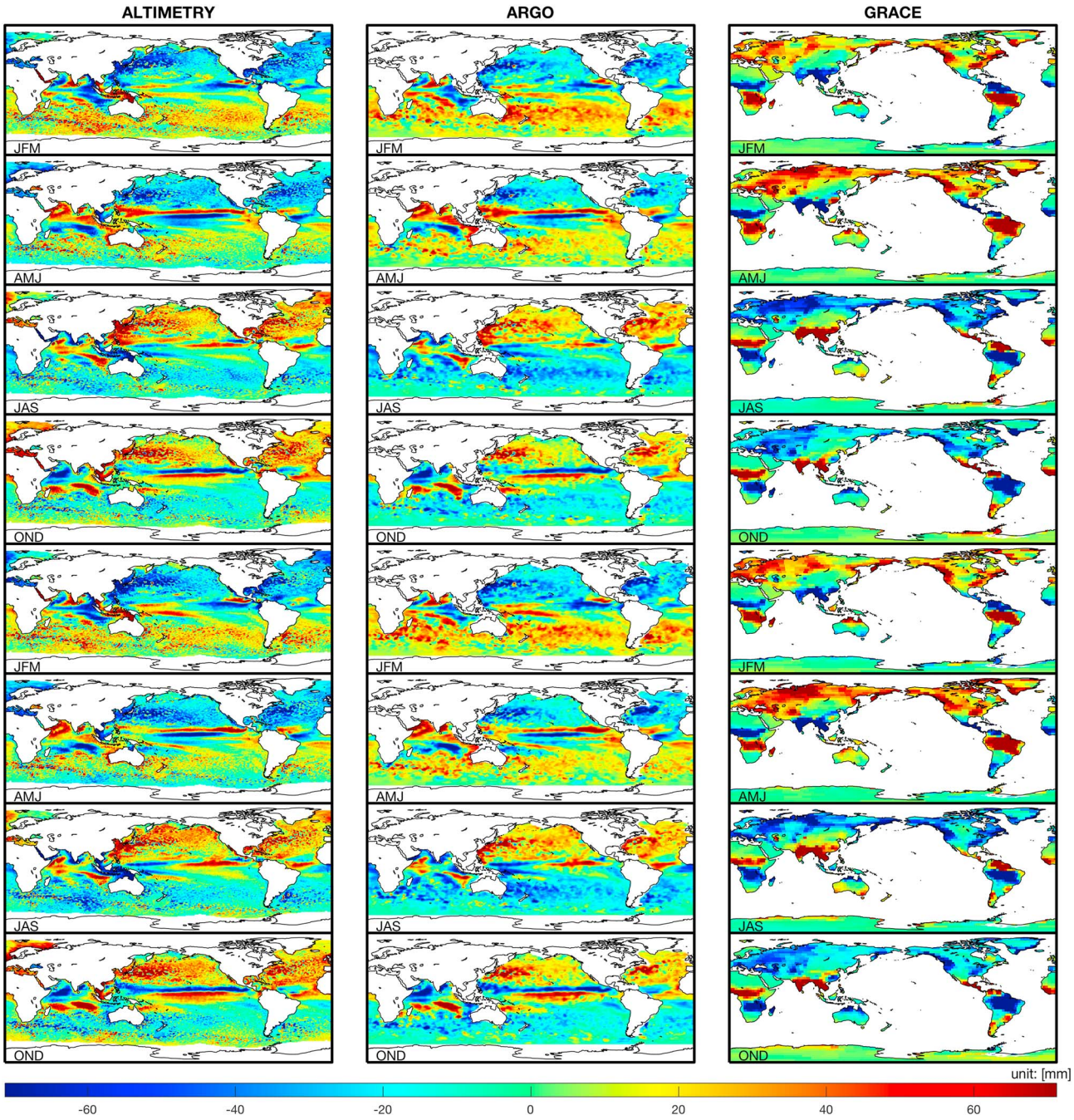

Figure 5. Second CSEOF mode from the combined decomposition representing the annual cycle in each of the three data sets. Seasonally averaged LVs are shown covering the 2-year nested period for altimetry (left), Argo (middle), and GRACE (right). CSEOF = cyclostationary empirical orthogonal function; LV = loading vector; GRACE = Gravity Recovery and Climate Experiment; JFM = January–March; AMJ = April–June; JAS = July–September; OND = October–December.

4.1.3. Higher Order Modes

A number of recent studies have discussed the impact of ENSO on global and regional sea level (Boening et al., 2012; Fasullo et al., 2013; Hamlington et al., 2016; Han et al., 2017; Zhang & Church, 2012). Indeed, the GMSL time series measured by satellite altimetry has a positive correlation with ENSO. In general, the warm phase of ENSO leads to an increase in global sea level on the order of several millimeters on intra-seasonal timescales and the cold phase leads to a decrease of similar magnitude on the same timescales. On the regional level, ENSO variability can lead to rises and falls on the order of tens of centimeters with the largest events causing shifts in coastal sea level that approach half a meter (e.g., in the tropical Pacific).

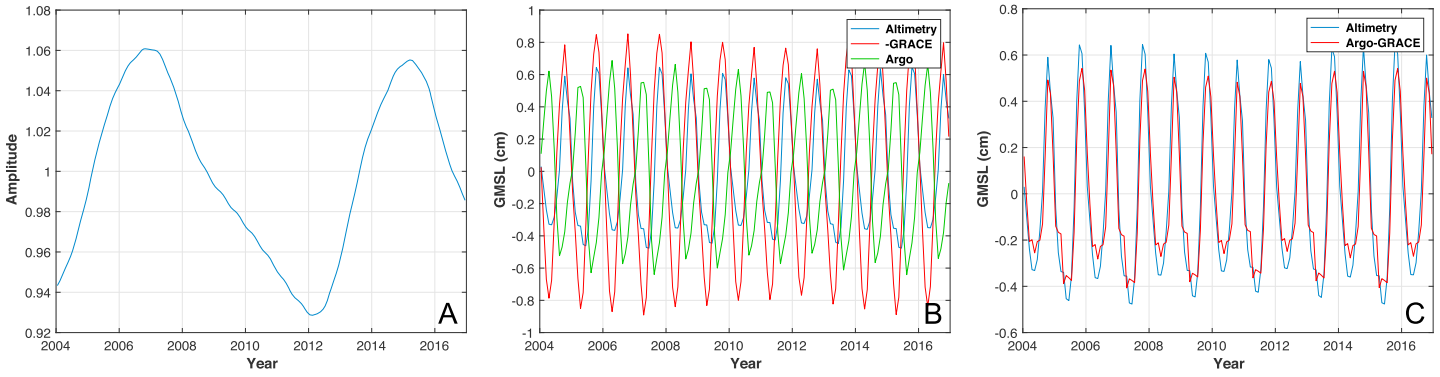

Figure 6. (a) PCTS associated with the annual mode in Figure 5 and (b) global mean time series computed by combining the CSEOF LV and PCTS and averaging spatially for each variable in the CSEOF annual mode. (c) The combination of Argo and GRACE compared to the total sea level measured by the altimetry. PCTS = principal component time series; CSEOF = cyclostationary empirical orthogonal function; LV = loading vector; GRACE = Gravity Recovery and Climate Experiment; GMSL = global mean sea level.

Two particular areas of focus of recent literature with regards to the impact of ENSO on sea level are (1) the relative contributions from steric and mass-driven sea level to sea level changes in response to ENSO events (e.g., Forget & Ponte, 2015; Piecuch & Quinn, 2016; Wu et al., 2017) and (2) the extent to which the response in sea level varies from event to event (Fasullo et al., 2013; Fasullo & Nerem, 2016). It has been argued that ENSO-related changes in GMSL are largely mass driven, associated with shifts in the hydrological cycle and changes in the patterns of precipitation and evaporation. On the other hand, Piecuch and Quinn (2016) performed a detailed analysis showing a significant portion of the signal associated with ENSO arises from steric variability. The sea level response to ENSO also appears to be nonlinear, with events noted as "large" by widely used climate indices not necessarily leading to a similarly large response in sea level. The opposite is also true, when a disproportionately large response to an ENSO event (when compared to an ENSO index) requires further explanation (e.g., Fasullo et al., 2013; Fasullo & Nerem, 2016). With regard to regional sea level, many of the studies mentioned above have used a variety of techniques to separate out the ENSO-related variability—including with CSEOFs—arriving at spatial patterns similar to the canonical ENSO pattern described by sea surface temperature.

One factor complicating the understanding of the sea level response to ENSO is the presence of similarly located decadal variability, including that often attributed to the PDO. The centers of variability for both climate modes are found in the Pacific Ocean, with the impacts on the climate system far reaching and varied. Unlike ENSO, the PDO is not particularly well-defined physically, with the original definition of the climate mode largely statistical in nature. Based on how they are computed, indices tracking ENSO and the PDO are correlated on intraseasonal timescales (e.g., Zhang & Church, 2012), leading to questions about where ENSO ends and where the variability associated with the PDO begins. Attempts at separating the two signals are made challenging due to the poor sampling of the relevant climate variables through the twentieth century and the relatively short satellite records that are only now approaching the length needed to begin to estimate decadal variability. Despite these challenges, PDO-related sea level has been a focus of many recent studies due largely to the large apparent impact on coasts around the Pacific Ocean.

Recent studies, particularly in Newman et al. (2016), have posited that the PDO is the expression of a combination of forcings rather than the result of a single process. In an attempt to be consistent with perhaps this explanation and understanding the limitations of our approach, we refer here to variability that would typically be attributed to the PDO as simply low-frequency variability. Furthermore, cognizant of the difficulty in separating low-frequency variability from ENSO in the 13-year record considered here, we avoid assigning definitive physical explanation to our statistical CSEOF modes and instead offer an interpretation of the explained variability and the potential impact of the short record on the returned modes.

4.1.3.1. Low-Frequency Mode

The third mode from the combined CSEOF analysis has an inherent timescale much longer than the 2-year nested period (Figure 7). Similar to the trend mode, the spatial patterns vary little over the course of the 2-year LV. Both the total and steric sea level LVs have a strong east-west dipole in the Pacific Ocean, with

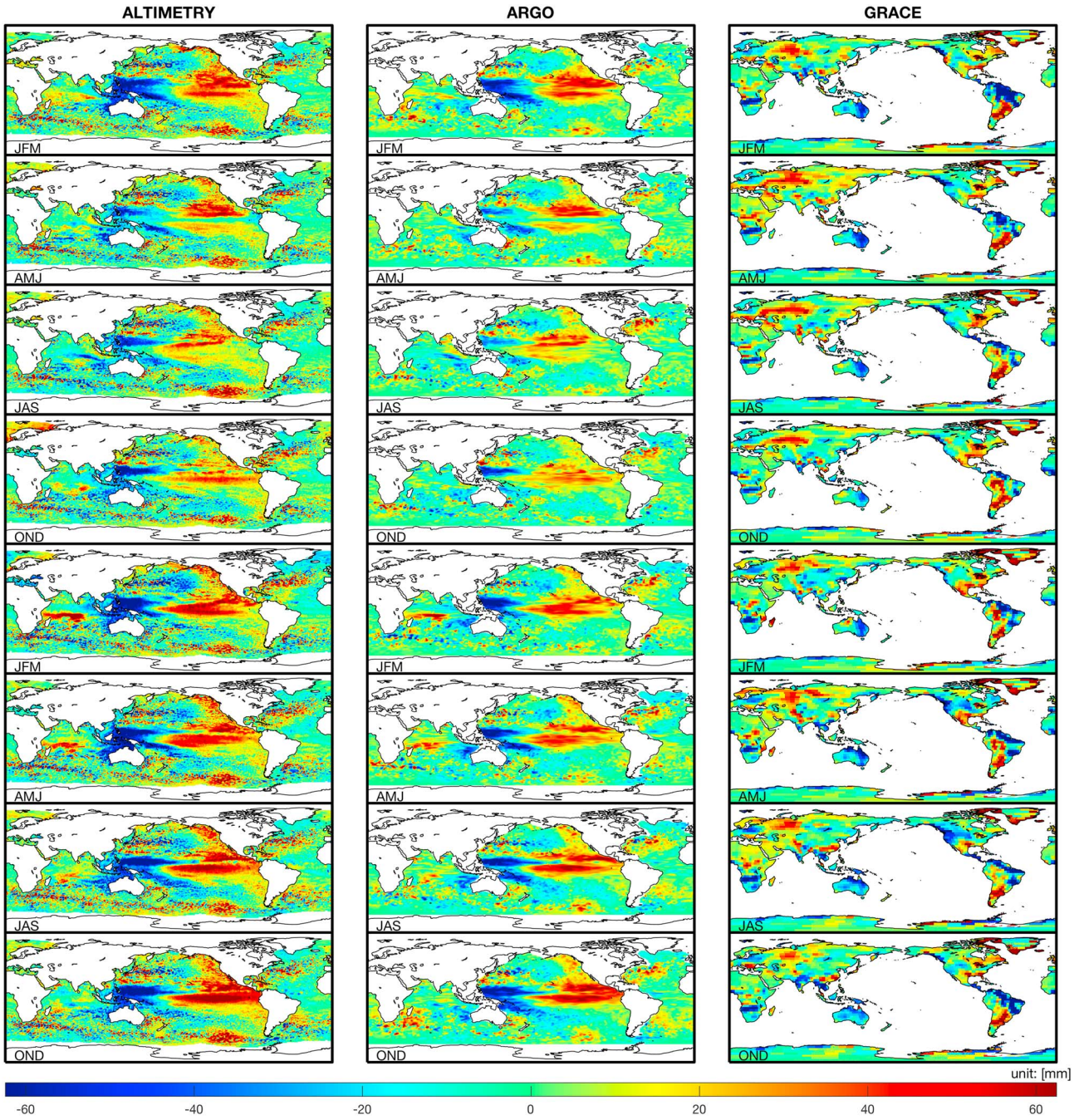

Figure 7. Third CSEOF mode from the combined decomposition representing the decadal (low frequency) variability in each of the three data sets. Seasonally averaged LVs are shown covering the 2-year nested period for altimetry (left), Argo (middle), and GRACE (right). CSEOF = cyclostationary empirical orthogonal function; LV = loading vector; GRACE = Gravity Recovery and Climate Experiment; JFM = January–March; AMJ = April–June; JAS = July–September; OND = October–December.

a similarly strong signal in the northeast Pacific that resembles the positive phase of the PDO in structure. Sea level signals in the Indian and Atlantic Oceans associated with this mode are not particularly prominent showing little persistent large-scale variability. On the other hand, there are a number of notable features in the TWS as measured by GRACE over this time period. In particular, the LV shows strong signals in eastern Australia, the Okavango Delta, southeastern United States, and much of South America, among others. This mode is in fact similar in its spatial variability to the decadal trend pattern extracted from much longer records of sea level, precipitation, and TWS in Hamlington et al. (2017). This

Figure 8. (a) PCTS associated with the low-frequency mode in Figure 7 and (b) global mean time series computed by combining the CSEOF LV and PCTS and averaging spatially for each variable in the CSEOF low-frequency mode. (c) The combination of Argo and GRACE compared to the total sea level measured by the altimetry. PCTS = principal component time series; CSEOF = cyclostationary empirical orthogonal function; LV = loading vector; GRACE = Gravity Recovery and Climate Experiment; GMSL = global mean sea level.

is further supported by the PCTS (Figure 8a) that shows a strong negative trend in the first half of the record —again, consistent with Hamlington et al. (2017)—before reversing in the latter half. Indeed, the change in trend seen in the PCTS around 2012 is in agreement with several other studies that identified a possible shift in decadal variability in the Pacific Ocean (e.g., Bromirski et al., 2011). To further investigate this low-frequency variability in TWS, a similar mode is extracted through the combined CSEOF analysis of GRACE land water storage and precipitation data from the Global Precipitation Climatology Project (Adler et al., 2003) from 2004 to 2016 (Figure 9). A CSEOF mode is returned with a similar spatial structure and PCTS to the GRACE mode in Figures 7 and 8a. The expression of this low-frequency variability differs in precipitation, however, and relationships between precipitation and TWS become apparent. For example, when this mode is in its negative phase, there is excess precipitation in eastern Australia during the austral summer before decreasing in the winter months. The TWS signal in GRACE, however, persists for the full year, consistent with the description of TWS in Australia in Fasullo et al. (2013). Other areas have a more direct connection, with TWS responding more quickly to an increase or decrease in precipitation. Such connections are difficult to observe in seasonally averaged maps, but in general, there is agreement between the LVs from GRACE TWS and precipitation as shown in Figure 9.

Further physical interpretation of this mode should be made with caution, but some speculation is offered here. Newman et al. (2016) discussed the PDO and Interdecadal Pacific Oscillation (IPO) in detail, concluding that the differences between the two are due to internal North Pacific processes and that the IPO is best described as the reddened ENSO component that is driven both by intraseasonal and decadal ENSO variability. In terms of the spatial pattern, the PDO has a stronger north Pacific signal and temporally correlates less highly with indices used to track ENSO than does the IPO. Given the global modes used here, it is likely that the low-frequency mode is best described as similar to the IPO, and the spatial pattern of the LVs—particularly those from steric and total sea level—appear to confirm this description albeit with a weaker than expected pattern in the southern Pacific. Furthermore, based on the consistency of the patterns in the LV, the common sign of the variability in the equatorial and tropical Pacific, and the slowly varying PCTS, we can conclude that this mode cannot be used to describe ENSO variability in general. Only time periods during which the north Pacific (or by extension the PDO) had the same phasing as ENSO could be explained by this mode. In other words, only an El Niño occurring during the positive phase of the PDO or a La Niña occurring during the negative phase of the PDO could be represented by the low-frequency mode. During the time period of study, this occurred during both during the 2010/2011 La Niña and the 2015/2016 El Niño. The fact that the LVs here require these events to persist for 2 years, however, does complicate the explanation that this mode simply explains when ENSO and the PDO/IPO are in phase. To demonstrate this further, we perform one additional check of this mode. We compute a 2-year CSEOF decomposition of northeast Pacific SST from the National Oceanic and Atmospheric Administration Optimum Interpolation Sea Surface Temperature v2 SST monthly fields. While the data set is available over the time period from 1981 to present, we use only the data covering the satellite altimeter time period, specifically

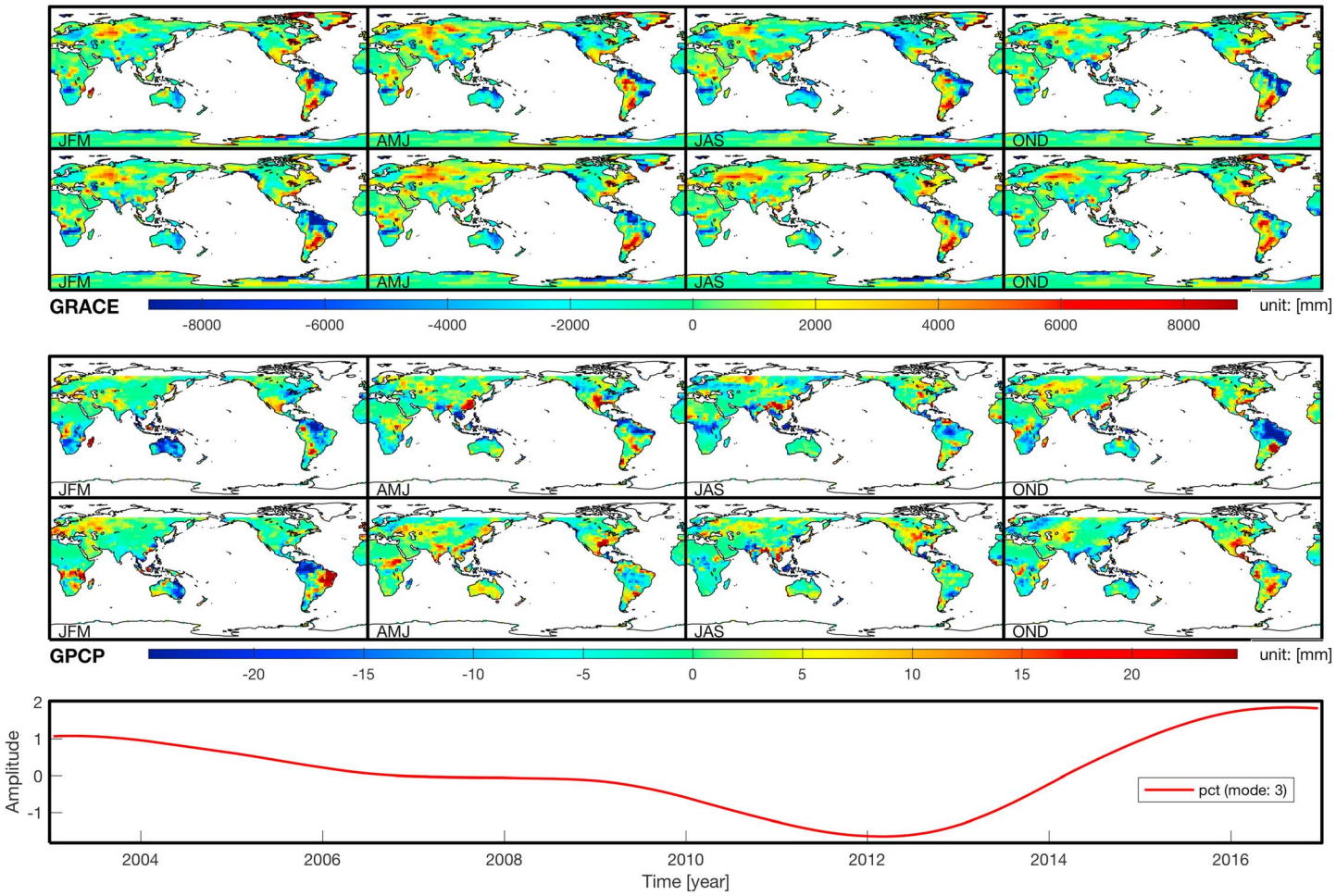

Figure 9. Combined CSEOF mode from analysis of GRACE land water storage and GPCP precipitation. As with the other combined analysis, this mode is the third after the trend and annual cycle. CSEOF = cyclostationary empirical orthogonal function; GRACE = Gravity Recovery and Climate Experiment; GPCP = Global Precipitation Climatology Project; JFM = January–March; AMJ = April–June; JAS = July–September; OND = October–December.

1993 through 2016 as with the other data sets. This data set is used only to validate the sea level modes. Following the regression technique of Hamlington et al. (2016), the total sea level CSEOFs from the combined analysis are regressed onto the dominant northeast Pacific SST mode. Specifically, CSEOFs are first computed from the northeast Pacific SST, with the dominant mode representing the widely used statistical description of the PDO typically obtained using EOFs. CSEOFs are then computed from the full global altimetry data set from 1993 to 2016. The returned PCTS are regressed onto the SST-computed PDO time series to obtain scaling coefficients. Finally, the altimetry LVs are multiplied by these scaling coefficients to create a corresponding sea level CSEOF LV that has the same temporal evolution as the SST PDO time series. The result is seen in Figure 10, with the PCTS from the SST and regression matching that of mode 3 (Figure 8a) very well during the overlapping time period. Further, the spatial patterns of the regressed CSEOF and combined CSEOF mode 3 also agree, suggesting a relationship between the variability commonly associated with the PDO and the low-frequency mode discussed here. In summary, it can be stated that this mode represents much of the decadal variability centered in the Pacific, but given the short record length, it is difficult to assess the degree to which intraseasonal ENSO variability is mixed in with the lower frequency signal.

Lastly, we can again examine the contribution of this mode to GMSL by combining the LVs with the PCTS and averaging spatially (Figures 8b and 8c). As a starting point, the combination of steric and mass-driven variability in this mode combine to match the total sea level response, achieving better correlation than the previous two modes. As discussed previously, the 2010/2011 La Niña and 2015/2016 El Niño appear to

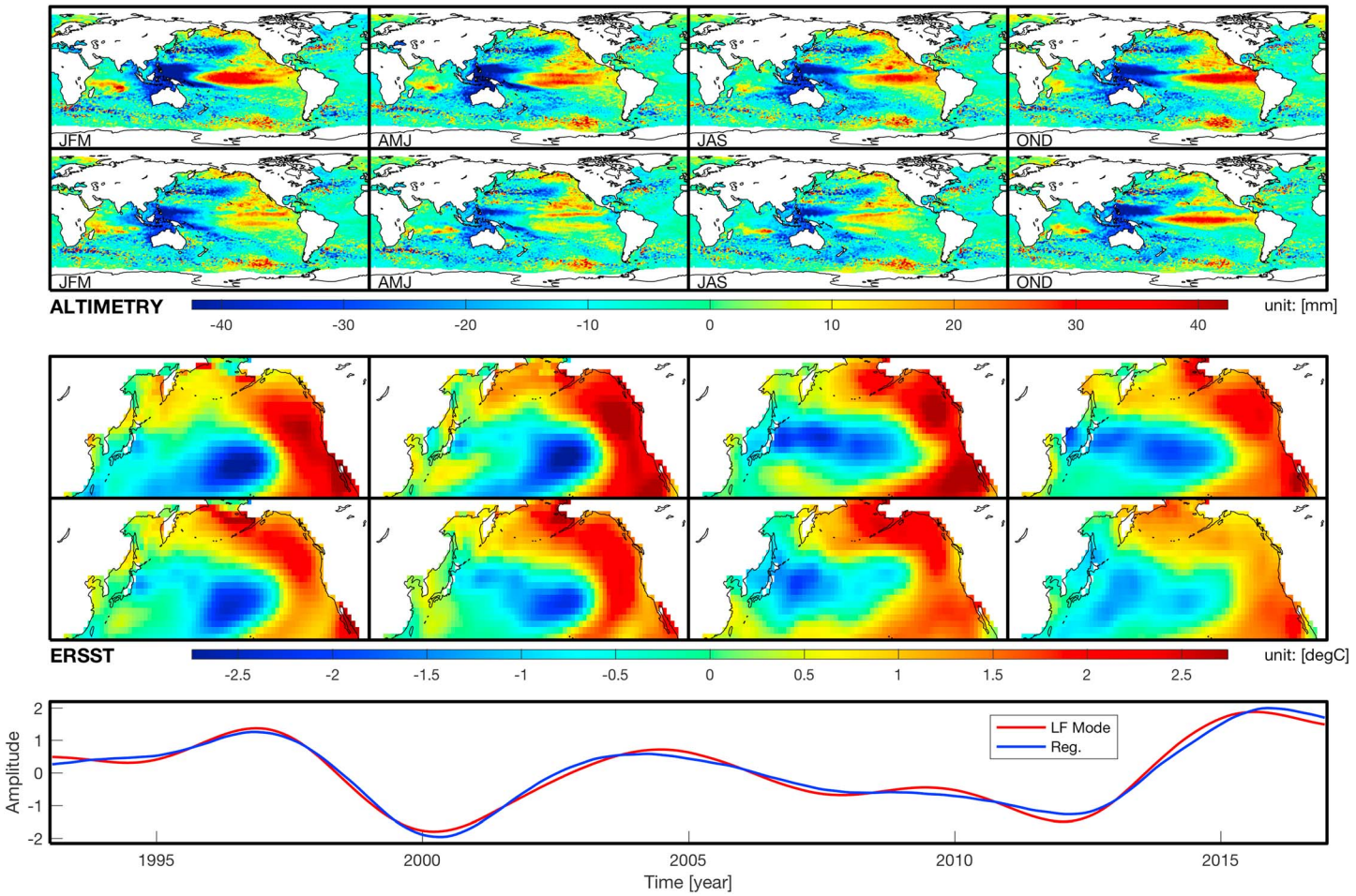

Figure 10. Regressed LVs from CSEOFs of altimetry data (top) onto the CSEOF of the North Pacific SST representing the PDO (middle). This regression is conducted over the time period from 1993 to 2016. The regressed (blue) and SST PDO PCTS (red) are also shown for comparison (bottom). LV = loading vector; CSEOF = cyclostationary empirical orthogonal function; SST = sea surface temperature; PDO = Pacific decadal oscillation; PCTS = principal component time series; ERSST = Extended Reconstructed Sea Surface Temperature; LF = low frequency; JFM = January–March; AMJ = April–June; JAS = July–September; OND = October–December.

be prominently featured in the GMSL time series. It is noteworthy, however, that the GMSL response to each event persists for an extended period of time, indicative of the slow-varying LVs in the mode. Furthermore, there appears to be a strong signal in both steric and mass-driven sea level, providing similar contributions to the change in GMSL and supporting the arguments made in Piecuch and Quinn (2016). Beyond the relative contributors, this mode does impart an acceleration to GMSL that could otherwise be misinterpreted as a long-term acceleration that would persist into the future, a possibility accounted for in Nerem et al. (2018).

4.1.3.2. Biennial Oscillation Mode

The final mode for discussion is the fourth from the combined CSEOF decomposition (Figure 11). This mode represents a biennial oscillation in ENSO, specifically the case when there is a year-to-year shift between the phases of ENSO. As described in Hamlington et al. (2016), this type of shift was particularly visible when the 1997/1998 El Niño was followed by a strong La Niña. During the record considered here, the 2009/2010 El Niño followed by the previously discussed La Niña is the most prominent occurrence of this type of variability, although a weaker phase transition over the period from 2012 to 2014 is also featured. Notably, this mode is near zero in recent years, during which a strong El Niño occurred. This is largely due to the persistent ENSO-like conditions from 2014 to 2016 that are not well explained by the biennial oscillation. Furthermore, there is only weak variability in the north Pacific in this mode, which is not representative of the higher sea level found in the region in recent years. Both the total sea level and steric sea level patterns agree well, while a number of areas around the globe are seen to undergo a 2-year oscillation in TWS.

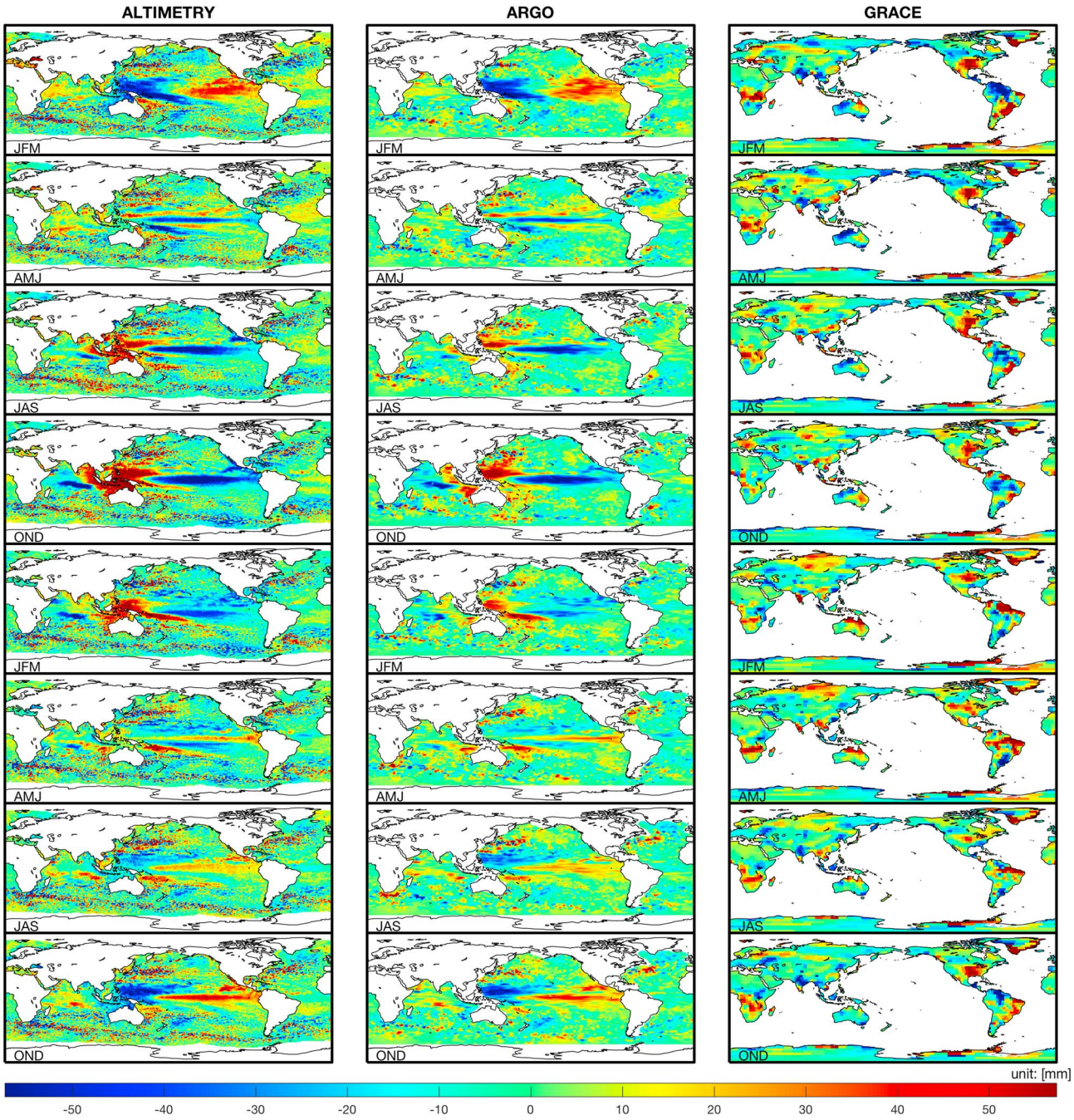

Figure 11. Fourth CSEOF mode from the combined decomposition representing the biennial variability in each of the three data sets. Seasonally averaged LVs are shown covering the 2-year nested period for altimetry (left), Argo (middle), and GRACE (right). CSEOF = cyclostationary empirical orthogonal function; LV = loading vector; GRACE = Gravity Recovery and Climate Experiment; JFM = January–March; AMJ = April–June; JAS = July–September; OND = October–December.

Particularly strong TWS signals are found in the central United States, northern and eastern Australia, and much of South America. When comparing the different variables, the LVs from GRACE do appear to lag the total and steric sea level signals by roughly a season. That is, the LV for GRACE does not weaken dramatically from 1 year into the next, while there is a large decline in the strength of the signal in the other two variables during the same seasonal shift. When considered in combination with the low-frequency mode from the previous section, these two modes describe much of the variability often associated with ENSO while also capturing decadal variability often associated with climate signals like the PDO and IPO.

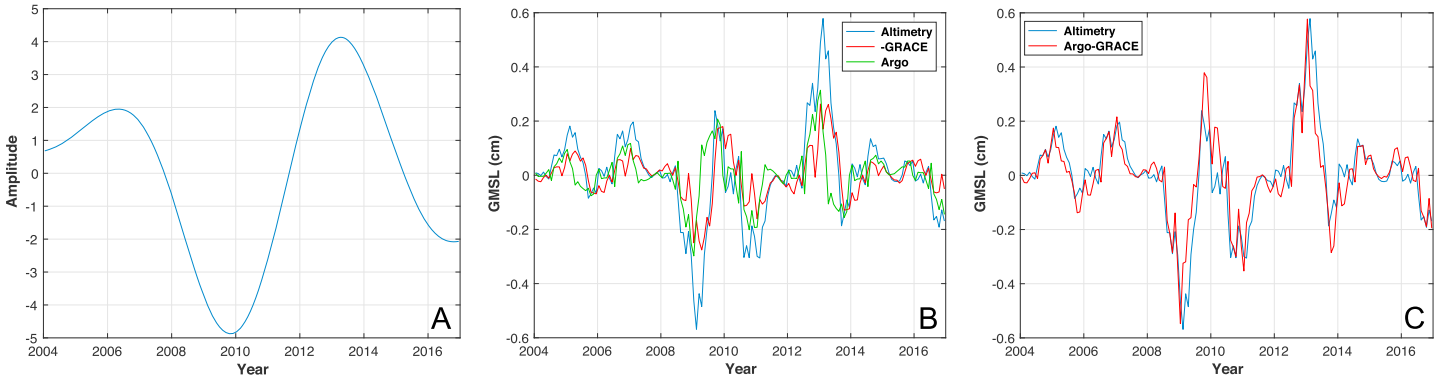

Figure 12. (a) PCTS associated with the biennial oscillation mode in Figure 11 and (b) global mean time series computed by combining the CSEOF LV and PCTS and averaging spatially for each variable in the CSEOF biennial mode. (c) The combination of Argo and GRACE compared to the total sea level measured by the altimetry. PCTS = principal component time series; CSEOF = cyclostationary empirical orthogonal function; LV = loading vector; GMSL = global mean sea level; GRACE = Gravity Recovery and Climate Experiment.

As a final step, the GMSL contribution is estimated and compared across the three variables considered here (Figure 12). Consistent with the previous mode, the combination of mass-driven and steric sea level combine to closely match the GMSL contribution in total sea level. There does, however, appear to be a lag in the relative contributions, with the steric response leading the mass-driven response by roughly a season. The low-frequency mode has a strong drop in GMSL of almost 6 mm from around the beginning of 2011 into 2012, while the biennial oscillation mode contributes a large decline in GMSL of similar magnitude from 2010 to 2011. When combined, these two modes explain the extended decline in GMSL from 2010 to 2012 that was the focus of discussion in both Boening et al. (2012) and Fasullo et al. (2013). There is a near-zero contribution to GMSL during the 2015/2016 El Niño.

5. Discussion

In this study, we attempt to find meaning in statistical modes and in many cases speculate on the nature of the variability that they contain. First, although it is important to physically understand rises and falls in sea level on all timescales, from a practical standpoint of planning for sea level rise at the coast, the most important number is the combined contribution of all sea level variability at a certain time in the future. As such, extracting the dominant modes of variability that are by definition those explaining the most variance, estimating their inherent timescales, and quantifying their impact on sea level change are worthwhile even if it is not possible to assign definitive physical meaning. Knowing that sea level in a particular part of the world has a strong decadal signal, for instance, is informative in the sense that we can expect similar decadal shifts in the future that will serve to suppress or exacerbate ongoing sea level rise. Second, even though the study and understanding of sea level is limited by the available observations, over the last couple of decades, we have had a vastly improved sea level observing system, owing largely to available satellite observations. Finding ways to take advantage of this observing system and leveraging the additional information can lead to new insights into the manner in which sea level changes and the relationship between sea level and other components of the climate system. Several studies have sought to find links between data from satellite altimeters, Argo floats, and GRACE, but here we attempt to connect these observations directly and search for the variability that is shared across the three data sets. Lastly, with relatively short modern records, it is useful to assess the extent to which we can understand and quantify the lower-frequency variability that may be present. This study investigates this in a comprehensive way and is potentially informative when attempting to extract ENSO-related variability from the GRACE record, for example.

In summary, there are a number of notable results from our combined CSEOF analysis:

1. The trends in total sea level, steric sea level, and land mass over the period from 2004 to 2016 are heavily influenced by natural variability. Given the record length, this is unsurprising, but the analysis conducted here does appear to separate much of the natural variability from the background trend that may be expected to persist into the future.

2. The strength of the annual cycle in sea level is shown to vary from year to year, albeit with relatively small deviations from the mean.
3. Decadal variability plays a large role in each of the three data sets, with the dominant signal appearing to explain both tropical and extratropical sea level variability. There is also a significant low-frequency signal in TWS, consistent in places with previously published literature.
4. Separating ENSO-related sea level from lower-frequency variability in the 13-year record remains challenging, and definitive attribution of shifts in regional and global sea level to a particular climate mode requires either further detailed investigation or a longer record.
5. There is great consistency between the measurements from the sea level observing system on a range of timescales, including intraseasonal to decadal as discussed here.

Each of the points above requires additional study, and further insight will likely be gained as the data records get longer (although with some gaps in data coverage). Further, much of the variability contained in the modes discussed here are ENSO-related and as a result Pacific dominated. Performing similar statistical analysis on individual basins could be very informative as recent studies have shown. By focusing on global modes, however, we emphasize that regional and global sea level are not independent and "regional" climate modes often have a significant global signal. As discussed above, many studies have focused on the regional and global relationship with regard to ENSO, but other climate signals, including the IPO/PDO, appear to have a similar nature. Finally, assessing how sea level is varying in the past decade can provide important insight into what may occur at the coast in the future. Studies such as this one underscore the need for continuity in the satellite records and at the very least, the need to maintain the current sea level observing system.

Acknowledgments
The satellite altimetry grids are available from NASA JPL/PO.DAAC at the following location: https://podaac.jpl.nasa.gov/dataset. GRACE land water storage data are available at http://grace.jpl.nasa.gov, supported by the NASA MEaSUREs Program. The gridded fields based on Argo data used to compute the steric sea level data are available at http://www.argo.ucsd.edu/Gridded_fields.html. The gridded fields based on Argo data used to compute the steric sea level data are available at http://www.argo.ucsd.edu/Gridded_fields.html. The research was carried out at the Jet Propulsion Laboratory, California Institute of Technology, under a contract with the National Aeronautics and Space Administration. B. D. H., F. W. L., J. T. R., and P. R. T. acknowledge support from NASA grant 80NSSC17K0564 (NASA Sea Level Change Team). C. G. P. acknowledges support from NSF awards OCE-1558966 and OCE-1834739. K. Y. K. was partially supported for this research by the National Science Foundation of Korea under the grant NRF- 2017R1A2B4003930.

References

Adler, R. F., Huffman, G. J., Chang, A., Ferraro, R., Xie, P. P., Janowiak, J., et al. (2003). The Version-2 Global Precipitation Climatology Project (GPCP) monthly precipitation analysis (1979–present). *Journal of Hydrometeorology*, *4*(6), 1147–1167. https://doi.org/10.1175/1525-7541(2003)004<1147:TVGPCP>2.0.CO;2

Alexander, M. A., Blade, I., Newman, M., Lanzante, J. R., Lau, N. C., & Scott, J. D. (2002). The atmospheric bridge: The influence of ENSO teleconnections on air-sea interaction over the global oceans. *Journal of Climate*, *15*(16), 2205–2231. https://doi.org/10.1175/1520-0442(2002)015<2205:TABTIO>2.0.CO;2

Ashok, K., Behera, S. K., Rao, S. A., Weng, H., & Yamagata, T. (2007). El Niño Modoki and its possible teleconnection. *Journal of Geophysical Research*, *112*, C11007. https://doi.org/10.1029/2006JC003798

Boening, C., Willis, J. K., Landerer, F. W., Nerem, R. S., & Fasullo, J. (2012). The 2011 La Niña: So strong, the oceans fell. *Geophysical Research Letters*, *39*, L19602. https://doi.org/10.1029/2012GL053055

Bromirski, P. D., Miller, A. J., Flick, R. E., & Auad, G. (2011). Dynamical suppression of sea level rise along the Pacific Coast of North America: Indications for imminent acceleration. *Journal of Geophysical Research*, *116*, C07005. https://doi.org/10.1029/2010JC006759

Calafat, F. M., Wahl, T., Lindsten, F., Williams, J., & Frajka-Williams, E. (2018). Coherent modulation of the sea-level annual cycle in the United States by Atlantic Rossby waves. *Nature Communications*, *9*(1), 2571. https://doi.org/10.1038/s41467-018-04898-y

Cazenave, A., Dieng, H.-B., Meyssignac, B., von Schuckmann, K., Decharme, B., & Berthier, E. (2014). The rate of sea-level rise. *Nature Climate Change*, *4*(5), 358–361. https://doi.org/10.1038/nclimate2159

Cazenave, A., Meyssignac, B., Ablain, M., Balmaseda, M., Bamber, J., Barletta, V., et al. (2018). Global sea-level budget 1993–present. *Earth System Science Data*, *10*(3), 1551–1590. https://doi.org/10.5194/essd-10-1551-2018

Deser, C., Phillips, A. S., & Hurrell, J. W. (2004). Pacific interdecadal climate variability: Linkages between the tropics and North Pacific during boreal winter since 1900. *Journal of Climate*, *17*(16), 3109–3124. https://doi.org/10.1175/1520-0442(2004)017<3109:PICVLB>2.0.CO;2

Dieng, H. B., Cazenave, A., Meyssignac, B., & Ablain, M. (2017). New estimate of the current rate of sea level rise from a sea level budget approach. *Geophysical Research Letters*, *44*, 3744–3751. https://doi.org/10.1002/2017GL073308

Fasullo, J. T., Boening, C., Landerer, F. W., & Nerem, R. S. (2013). Australia's unique influence on global sea level in 2010–2011. *Geophysical Research Letters*, *40*, 4368–4373. https://doi.org/10.1002/grl.50834

Fasullo, J. T., & Nerem, R. S. (2016). Interannual variability in global mean sea level estimated from the CESM large and last millennium ensembles. *Water*, *8*(11), 491. https://doi.org/10.3390/w8110491

Forget, G., & Ponte, R. M. (2015). The partition of regional sea level variability. *Progress in Oceanography*, *137*, 173–195. https://doi.org/10.1016/j.pocean.2015.06.002

Gill, A. E., & Niiler, P. P. (1973). The theory of the seasonal variability in the ocean. *Deep Sea Research*, *20*, 141–177.

Hamlington, B. D., Cheon, S. H., Thompson, P. R., Merrifield, M. A., Nerem, R. S., Leben, R. R., & Kim, K.-Y. (2016). An ongoing shift in pacific ocean sea level. *Journal of Geophysical Research: Oceans*, May, *121*, 5084–5097. https://doi.org/10.1002/2016JC011815

Hamlington, B. D., Leben, R. R., Kim, K.-Y., Nerem, R. S., Atkinson, L. P., & Thompson, P. R. (2015). The effect of the El Niño-Southern Oscillation on US regional and coastal sea level. *Journal of Geophysical Research: Oceans*, *120*, 3970–3986. https://doi.org/10.1002/2014JC010602

Hamlington, B. D., Leben, R. R., Nerem, R. S., & Kim, K.-Y. (2011). The effect of signal-to-noise ratio on the study of sea level trends. *Journal of Climate*, *24*(5), 1396–1408. https://doi.org/10.1175/2010JCLI3531.1

Hamlington, B. D., Leben, R. R., Strassburg, M. W., Nerem, R. S., & Kim, K.-Y. (2013). Contribution of the Pacific Decadal Oscillation to global mean sea level trends. *Geophysical Research Letters*, *40*, 5171–5175. https://doi.org/10.1002/grl.50950

Hamlington, B. D., Reager, J. T., Lo, M.-H., Karnauskas, K. B., & Leben, R. R. (2017). Separating decadal global water cycle variability from sea level rise. *Scientific Reports*, *7*(1), 995. https://doi.org/10.1038/s41598-017-00875-5

Hamlington, B. D., Strassburg, M. W., Leben, R. R., Han, W., Nerem, R. S., & Kim, K.-Y. (2014). Uncovering an anthropogenic sea-level rise signal in the Pacific Ocean. *Nature Climate Change*, *4*(9), 782–785. https://doi.org/10.1038/nclimate2307

Han, W., Meehl, G., Stammer, D., Hu, A., Hamlington, B., Kenigson, J., et al. (2017). Spatial patterns of sea level variability associated with natural internal climate modes. *Surveys in Geophysics*, *38*(1), 217–250. https://doi.org/10.1007/s10712-016-9386-y

Kenigson, J. S., & Han, W. (2018). Decadal shift in NAO-linked interannual sea level variability along the U.S. northeast coast. *Journal of Climate*, *31*(13), 4981–4989. https://doi.org/10.1175/JCLI-D-17-0403.1

Kim, K.-Y., Hamlington, B. D., & Na, H. (2015). Theoretical foundation of CSEOF analysis for geophysical and climatic variables: Concepts and examples. *Earth-Science Reviews*, *150*, 201–218. https://doi.org/10.1016/j.earscirev.2015.06.003

Leuliette, E. W., & Willis, J. K. (2015). Balancing the sea level budget. *Oceanography*, *24*(2), 122–129.

Mantua, N. J., & Hare, S. R. (2002). The Pacific Decadal Oscillation. *Journal of Oceanography*, *58*(1), 35–44. https://doi.org/10.1023/A:1015820616384

Mason, S. A., Hamlington, P. E., Hamlington, B. D., Jolly, W. M., & Hoffman, C. M. (2017). Effects of climate oscillations on wildland fire potential in the continental United States. *Geophysical Research Letters*, *44*, 7002–7010. https://doi.org/10.1002/2017GL074111

Moon, J.-H., Song, Y. T., Bromirski, P. D., & Miller, A. J. (2013). Multi-decadal regional sea level shifts in the Pacific over 1958–2008. *Journal of Geophysical Research: Oceans*, *118*, 7024–7035. https://doi.org/10.1002/2013JC009297

Moon, J.-H., Song, Y. T., & Lee, H. (2015). PDO and ENSO modulations intensified decadal sea level variability in the tropical Pacific. *Journal of Geophysical Research: Oceans*, *120*, 8229–8237. https://doi.org/10.1002/2015JC011139

Nerem, R. S., Beckley, B. D., Fasullo, J. T., Hamlington, B. D., Masters, D., & Mitchum, G. T. (2018). Climate-change-driven accelerated sea level rise detected in the altimeter era. *PNAS*, *115*(9), 2022–2025. https://doi.org/10.1073/pnas.1717312115

Newman, M., Alexander, M. A., Ault, T. R., Cobb, K. M., Deser, C., di Lorenzo, E., et al. (2016). The Pacific Decadal Oscillation, revisited. *Journal of Climate*, *29*(12), 4399–4427. https://doi.org/10.1175/JCLI-D-15-0508.1

Newman, M., Compo, G. P., & Alexander, M. A. (2003). ENSO-forced variability of the Pacific decadal oscillation. *Journal of Climate*, *16*(23), 3853–3857. https://doi.org/10.1175/1520-0442(2003)016<3853:EVOTPD>2.0.CO;2

Palanisamy, H., Meyssignac, B., Cazenave, A., & Delcroix, T. (2015). Is anthropogenic sea level fingerprint already detectable in the Pacific Ocean. *Environmental Research Letters*, *10*(8). https://doi.org/10.1088/1748-9326/10/8/084024

Piecuch, C. G., & Quinn, K. J. (2016). El Niño, La Niña, and the global sea level budget. *Ocean Science*, *12*(6), 1165–1177. https://doi.org/10.5194/os-12-1165-2016

Reager, J. T., Gardner, A. S., Famiglietti, J. S., Wiese, D. N., Eicker, A., & Lo, M.-H. (2016). A decade of sea level rise slowed by climate-driven hydrology. *Science*, *351*(6274), 699–703. https://doi.org/10.1126/science.aad8386

Rodell, M., Famiglietti, J. S., Wiese, D. N., Reager, J. T., Beaudoing, H. K., Landerer, F. W., & Lo, M.-H. (2018). Emerging trends in global freshwater availability. *Nature*, *557*(7707), 651–659. https://doi.org/10.1038/s41586-018-0123-1

Roemmich, D., & Gilson, J. (2009). The 2004–2008 mean and annual cycle of temperature, salinity, and steric height in the global ocean from the Argo program. *Progress in Oceanography*, *82*(2), 81–100. https://doi.org/10.1016/j.pocean.2009.03.004

Sagi, N. H., & Yamagata, T. (2003). Possible impacts of Indian Ocean Dipole mode on global climate. *Climate Research*, *25*(2), 151–169.

Sreenivas, P., Gnanaseelan, C., & Prasad, K. V. S. R. (2012). Influence of El Niño and Indian Ocean dipole on sea level variability in the Bay of Bengal. *Global and Planetary Change*, *80-81*, 215–225. https://doi.org/10.1016/j.gloplacha.2011.11.001

Timmermann, A., An, S.-Il, Kug, J.-S., Jin, F.-F., Cai, W., Capotondi, A., et al. (2018). El Niño–Southern Oscillation complexity. *Nature*, *559*, 535–545.

Watkins, M., & Yuan, D. (2012). JPL Level-2 processing standards document for product release 05 GRACE 327-742, revision 5.0.

Wiese, D. N., Landerer, F. W., & Watkins, M. M. (2016). Quantifying and reducing leakage errors in the JPL RL05M GRACE mascon solution. *Water Resources Research*, *52*, 7490–7502. https://doi.org/10.1002/2016WR019344

Wu, Q., Zhang, X., Church, J. A., & Hu, J. (2017). Variability and change of sea level and its components in the Indo-Pacific region during the altimetry era. *Journal of Geophysical Research: Oceans*, *122*, 1862–1881. https://doi.org/10.1002/2016JC012345

Yeo, S.-R., & Kim, K.-Y. (2013). Global warming, low-frequency variability, and biennial oscillation: An attempt to understand the physical mechanisms driving major ENSO events. *Climate Dynamics*, *43*(3–4), 771–786. https://doi.org/10.1007/s00382-013-1862-1

Zhang, X., & Church, J. A. (2012). Sea level trends, interannual and decadal variability in the Pacific Ocean. *Geophysical Research Letters*, *39*, L21701. https://doi.org/10.1029/2012GL053240